

Copper bis(thiosemicarbazone) Complexes with Pendent Polyamines: Effects of Proton Relays and Charged Moieties on Electrocatalytic HER

Caleb A. Calvary, [a] Oleksandr Hietsoi, [a, b] Dillon T. Hofsommer, [a] Henry C. Brun, [a] Alison M. Costello, [a] Mark S. Mashuta, [a] Joshua M. Spurgeon, [c] Robert M. Buchanan, *[a] and Craig A. Grapperhaus*[a]

A series of new bis(thiosemicarbazonato) Cu(II) complexes with pendent polvamines, diacetyl-(N, -dimethylethylenediaminothiosemicarbazonato)-(N'-methyl-3-thio-semicarbazonato)butane-2,3-diimine)-copper(II) (Cu-1), diacetyl-bis (N-dimethylethylenediamino-3-thiosemicarbazonato)butane-2,3-diimine)-copper(II) (Cu-3), and their cationic derivatives Cu-2 and Cu-4, have been synthesized and fully characterized by spectroscopic, electrochemical, and X-ray diffraction methods. Complexes Cu-1-Cu-4 are analogues of Cu(ATSM), which contains a similar N₂S₂ donor core with terminal non-coordinating amines. Substitution of the methyl group(s) of the terminal amines of H₂ATSM with N,N-dimethylethylenediamine followed by alkylation generates a charged quaternary amine in the ligand framework. The charged site tunes the redox potentials of the complexes with minimal changes in their physical and electronic properties. The HER activity of all four copper complexes were evaluated in acetonitrile with glacial acetic acid. All of the complexes have lower HER overpotentials than Cu(ATSM), which is attributed to charge effects. The pendent amines of **Cu-1** and **Cu-3** have the lowest HER overpotential as the pendent tertiary amine also serves as a proton relay to enhance proton rearrangement under catalytic conditions. Complex **Cu-3** showed the highest activity with a TOF of $12 \times 10^3 \, \mathrm{s}^{-1}$, an overpotential of 0.65 V, and faradaic efficiency of 100%.

Introduction

The metal-centered and ligand-centered reduction potentials of molecular catalysts can be tuned through substituent effects by employing electron-donating or electron-withdrawing groups.^[1-3] For electrocatalysts, changing the electronic structure directly influences overpotential and the turnover frequency (TOF) of catalysis.^[4-6] The tuning of electrocatalysts using "through-structure" (electronic, inductive or resonant) and "through-space" (electrostatic and hydrogen bonding) substituent effects was exquisitely demonstrated by Constentin, Robert, and Savéant through a series of groundbreaking

studies.[4,7-9] The through-structure effects displayed opposing outcomes as factors that reduced overpotential also decreased turnover frequency (TOF) and vice versa.^[7] This trend is also well documented in electrocatalysts for the hydrogen evolution reaction (HER).[10] In contrast, through-space substituent effects provide a means to both lower the overpotential and increase TOF.[11] The effect of through-space interactions on electrocatalysis has also been evaluated through the introduction of a secondary coordination sphere. [9,10,12,13] Ligands with bulky groups, fixed charge sites, and hydrogen-bonding proton relay pendents are of growing interest as they may play an important role in generating and stabilizing reactive intermediates during catalysis. [9,14] For example, incorporation of charged groups in the second coordination sphere, as part of the ligand framework or as appended groups, have been shown to reduce the reduction potential of the complex via through-space interactions.[11,14]

Several bis(thiosemicarbazone) (BTSC) metal complexes, including derivatives of diacetyl-bis(N-methyl-3-thiosemicarbazone) (H₂ATSM), have been evaluated as hydrogen evolution reaction (HER) electrocatalysts. The BTSC ligands are non-innocent with HER mechanisms following *ligand-assisted metal-centered*, *ligand-centered*, or *metal-assisted ligand-centered* pathways depending on the identity of the metal. For example, Ni derivatives follow a *ligand-assisted metal-centered* pathway in which the ligand serves as an electron reservoir on the pathway to a putative Ni(III)-hydride intermediate. In contrast, Cu (ATSM) follows a *ligand-assisted metal-centered* pathway in which initial metal-centered reduction is followed by ligand-

[a] C. A. Calvary, Prof. O. Hietsoi, Dr. D. T. Hofsommer, H. C. Brun, A. M. Costello, Dr. M. S. Mashuta, Prof. Dr. R. M. Buchanan, Prof. Dr. C. A. Grapperhaus Department of Chemistry, University of Louisville 2320 South Brook Street, Louisville, KY 40292, USA E-mail: robert.buchanan@louisville.edu craig.grapperhaus@louisville.edu

https://louisville.edu/faculty/cagrap01
[b] Prof. O. Hietsoi
Department of Chemistry,
Middle Tennessee State University,

Murfreesboro, TN 37132, USA

[c] Prof. Dr. J. M. Spurgeon Conn Center for Renewable Energy Research, University of Louisville, Louisville, KY 40292, USA

Supporting information for this article is available on the WWW under https://doi.org/10.1002/ejic.202000774



based protonation and reduction events with evolution of H_2 from the ligand-center.^[22]

Recently, we evaluated second coordination sphere effects of flexible pendent polyamines on the HER activity of a series of BTSC Ni(II) complexes (Scheme 1).^[14] Complexes Ni-1 and Ni-3 contained basic, tertiary amines that were protonated under catalytic conditions and Ni-2 and Ni-4 are their methylated, quaternary amine derivatives. While all of the complexes have the same charge under catalytic conditions, only Ni-1 and Ni-3 displayed a decreased overpotential relative to Ni(ATSM). This was attributed to the participation of the pendent amine as a proton relay, which facilitated formation of the Ni(III)-hydride intermediate. Herein, we extend the study to evaluate the related Cu complexes Cu-1-Cu-4.

Results and Discussion

Synthesis and Characterization

The ligands H_2L^1 and H_2L^2 were prepared via transamination of diacetyl-N,N-dimethyl-N'-methylbis(thiosemicarbazone) and diacetyl-bis(N,N-dimethylthiosemicarbazone), respectively, with N,N-dimethylethylenediamine as previously described. Metalation of H_2L^1 with copper(II) acetate tetrahydrate in methanol at room temperature yielded **Cu-1**. Complex **Cu-3** was obtained upon reflux of a methanol solution containing H_2L^2 and copper (II) acetylacetonate. The N-methylated derivatives **Cu-2** and **Cu-4** were produced by alkylation of **Cu-1** and **Cu-3**, respectively, with methyl iodide. For **Cu-2**, metathesis of the iodide with hexafluorophosphate yielded the N-methylated derivative **Cu-2***. The infrared spectra of ligands H_2L^1 and H_2L^2 display N-H stretches between 3337 and 3364 cm⁻¹ that are lost upon metal complexation (Figures S7-S12).

The electronic spectra of **Cu-1–Cu-4** recorded in acetonitrile display ligand to metal charge transfer bands near 460 nm (Figure S13). All four complexes display a more intense ligand to ligand charge transfer band near 320 nm. Two additional bands are observed for **Cu-2** and **Cu-4** at 220 nm and 225 nm, respectively. The EPR spectra of **Cu-1–Cu-4** were recorded in frozen DMF solution at 77 K (Figures S18–21). The **Cu-1** complex displays an axial signal with $g_{\parallel} = 2.11$, $g_{\perp} = 2.01$, and $A_{\parallel} = 191$ G consistent with square planar Cu(II) and a single unpaired

M = Ni, Cu

M-3: R = N(CH₃)₂, M-4: R = N(CH₃)₃

Scheme 1. Metal bis(thiosemicarbazone) complexes M(ATSM) and M-1-M-4.

electron located in d_{x2-y2} orbital. Complexes **Cu-2–Cu-4** display spectra with similar parameters. The g-values and coupling constant are in agreement with those reported for other Cu (BTSC) complexes.^[23]

X-ray quality single crystals of Cu-1–Cu-3 were obtained by slow evaporation of organic solutions. Crystals of Cu-4 were twinned and refined as described in the experimental section. Crystal data and structure refinement details for all complexes are listed in Table 1. All compounds crystallize as discrete, square planar Cu(II) complexes. Complexes Cu-2 and Cu-4 contain one water molecule in the crystal lattice. Selected bond distances and angles are summarized in Table 2. Overall, complexes Cu-1–Cu 4 display the same general coordination environment as their nickel analogs with similar bond angles around the metal center and slightly longer (~0.1 Å) metalligand bond distances.^[14]

Orange plate single crystals of **Cu-1** were obtained by slow evaporation of a 1:1 MeCN/EtOH solution of **Cu-1** and crystallizes in the orthorhombic space group *P*bca. The asymmetric unit consists of one equivalent of **Cu-1** (Figure 1). The N₂S₂ coordination environment is square planar, and the Cu–N1, Cu–N3, Cu–S1, and Cu–S2 bond distances are 1.967(2), 1.960(2), 2.2394(7) and 2.2392(8) Å, respectively. The S1–C5, N1–N2 and C1–C2 bond distances of 1.766(3), 1.375(3), and 1.475(4) Å, respectively, are typical of C–S, N–N, and C–C single bonds. The shorter N1–C1 and N2–C5 bond distances of 1.294(3) and 1.323(4) Å, respectively, reveal C=N bond character. In general, the bond distances and bond angles for **Cu-1** are similar to the parent Cu(ATSM) complex.^[24]

Single crystals of **Cu-2** were isolated as red-brown plates by slow evaporation of a 1:1 MeCN/EtOH solution of **Cu-2**. The complex crystallizes in the monoclinic space group $P2_1/n$, and the asymmetric unit consists of one molecule of **Cu-2**, an iodide ion and one water molecule of hydration (Figure 2). The iodide and water are hydrogen-bonded to the pendent nitrogen atoms N6 and N5, respectively, forming a network of symmetry generated metal complexes (Figure S26). As observed for **Cu-1**, the CuN₂S₂ unit is square planar and has similar metal-ligand bond distances (Table 2).

Complex Cu-3 was isolated as red-brown prisms by vapor diffusion of Et_2O into a MeCN solution of Cu-3. The complex crystallizes in the triclinic space group P-1, and the asymmetric unit consists of one molecule of Cu-3. (Figure 3). Bond distances

Figure 1. ORTEP view (50% probability ellipsoids) of **Cu-1** showing atom labelling for all non-hydrogen atoms in the asymmetric unit.



Identification code	Cu-1	Cu-2	Cu-3	Cu-4
Empirical formula	$C_{11}H_{21}CuN_7S_2$	C ₁₂ H ₂₄ CuN ₇ S ₂ ,H ₂ O,I	C ₁₄ H ₂₈ CuN ₈ S ₂	C ₁₆ H ₃₄ CuN ₈ S ₂ ,H ₂ O,2I
CCDC number	2013250	2013252	2013249	2013251
Formula weight	379.01	538.96	436.10	737.99
Temperature (K)	101.95(10)	102.05(10)	102(3)	101.9(2)
Wavelength (Å)	0.71073	0.71073	0.71073	0.71073
Crystal system	Orthorhombic	Monoclinic	Triclinic	Triclinic
Space group	<i>P</i> bca	<i>P</i> 2₁/n	P-1	P-1
Unit cell dimensions		•		
a (Å)	10.6564(4)	8.2819(4)	8.8712(3)	9.3519(5)
b (Å)	15.0501(6)	29.944(2)	9.1946(3)	9.7849(4)
c (Å)	20.1476(8)	8.9097(4)	12.8507(3)	15.2845(8)
α (deg)	90	90	95.544(2)	85.659(4)
β (deg)	90	115.093(6)	106.566(3)	73.253(4)
γ (deg)	90	90	107.451(3)	81.935(4)
V (Å ³)	3231.3(2)	2001.03(19)	939.24(5)	1325.16(11)
Z	8	4	2	2
$d_{\text{calcd}} \text{ (Mg/m}^3\text{)}$	1.558	1.789	_ 1.542	1.850
Absorption coefficient (mm ⁻¹)	1.614	2.858	1.401	3.335
F(000)	1576	1076	458	726
Crystal color, habit	orange plate	red-brown plate	red-brown prism	orange needle
Crystal size (mm³)	0.20×0.20×0.01	0.42×0.20×0.05	0.30×0.17×0.05	0.40×0.03×0.01
θ range for data collection (deg)	3.38 to 27.22	3.25 to 33.60	3.38 to 30.18	3.30 to 27.34
Index ranges	-13 < h < 13	-12 < h < 12	-12 < h < 12	-12 < h < 12
acx ranges	-16 < k < 16	-46 < k < 46	-13 < k < 13	$-12 \le k \le 12$
	-25 < I < 25	-13 < <i>l</i> < 13	-18 < <i>l</i> < 18	-19 < <i>l</i> < 19
Reflections collected	16683	33362	27814	11440
Independent reflections	3600 [R(int) = 0.0603]	7885 [R(int) = 0.0348]	5554 [R(int) = 0.0326]	11440 [R(int) = 0.0000]
Completeness to theta max (%)	99.8	99.6	99.9	99.5
Absorption correction	multi-scan	multi-scan	multi-scan	multi-scan
Max. and min transmission	1.000 and 0.928	1.000 and 0.624	1.000 and 0.922	1.000 and 0.796
Refinement method	full-matrix least-squares on	full-matrix least-squares on	full-matrix least-squares on	full-matrix least-squares on
nemenen memoa	F ²	F ²	F ²	F ²
Data/restrains/parameters	3600/0/274	7885/0/305	5554/0/338	11440/3/293
Goodness of fit on F^2	1.078	1.078	1.050	1.133
Final R indices $[I > 2\sigma(I)]^{[a,b]}$	R1 = 0.0404,	R1 = 0.0289,	R1 = 0.0234,	R1 = 0.0733,
a	wR2=0.0765	wR2 = 0.0564	wR2=0.0539	wR2=0.1736
R indices (all data) ^[a,b]	R1 = 0.0641,	R1 = 0.0392,	R1 = 0.0279,	R1 = 0.0993,
A marces (an data)	wR2=0.0849	WR2 = 0.0600	WR2 = 0.0564	wR2=0.1833
Largest diff. peak and hole	0.544 and -0.498	1.065 and -0.666	0.449 and -0.317	4.067 and -1.658

[a] R1 = $\Sigma ||F_o|| - |F_c||/\Sigma |F_o|$. [b] wR2 = $\{\Sigma [w(F_o^2 - F_c^2)^2]/\Sigma [w(F_o^2)^2]\}^{1/2}$, where $w = q/\sigma^2(F_o^2) + (qp)^2 + \text{bp. GOF} = S = \{\Sigma [w(F_o^2 - F_c^2)^2]/(n-p)\}^{1/2}$, where n is the number of reflections and p is the number of parameters refined.

Table 2. Selected bond distances (Å) and angles (deg) for Cu-1–Cu-4.				
	Cu-1	Cu-2	Cu-3	Cu-4
Cu1-N1	1.967(2)	1.9732(13)	1.9820(10)	1.966(6)
Cu1-N3	1.960(2)	1.9562(14)	1.9647(11)	1.956(6)
Cu1-S1	2.2394(7)	2.2574(5)	2.2650(3)	2.258(2)
Cu1-S2	2.2392(8)	2.2709(4)	2.2929(3)	2.267(2)
S1–C5	1.766(3)	1.7615(16)	1.7555(13)	1.755(7)
S2C6	1.753(3)	1.7491(17)	1.7575(12)	1.762(7)
N1C1	1.294(3)	1.300(2)	1.3007(16)	1.284(10)
N1-N2	1.375(3)	1.3626(19)	1.3701(14)	1.359(9)
N2C5	1.323(4)	1.326(2)	1.3284(16)	1.304(10)
N3C2	1.296(3)	1.298(2)	1.2979(16)	1.276(10)
N3-N4	1.368(3)	1.3618(19)	1.3703(14)	1.360(9)
N4C6	1.336(3)	1.324(2)	1.3199(16)	1.316(10)
C1–C2	1.475(4)	1.474(2)	1.4756(16)	1.474(11)
N3Cu1N1	80.65(9)	80.02(6)	80.22(4)	79.1(3)
N3–Cu1–S1	165.89(7)	163.91(4)	157.97(3)	164.25(19)
N1–Cu1–S1	85.25(7)	84.70(4)	83.65(3)	85.14(19)
N3–Cu1–S2	85.62(7)	85.24(4)	83.70(3)	85.03(19)
N1–Cu1–S2	165.52(7)	164.14(4)	162.39(3)	163.59(19)
S1–Cu1–S2	108.47(3)	109.343(16)	109.740(12)	110.67(8)

and angles for **Cu-3** are listed in Table 2. Orange needle crystals of **Cu-4** were obtained by slow evaporation of MeCN solution of **Cu-4**. The complex crystallizes in the triclinic space group *P*–1 containing one cation of **Cu-4**, two iodides and one water of hydration per asymmetric unit (Figure 4). The iodide anions I1 and I2 are hydrogen-bonded to the pendent nitrogen atoms N7 and N5, respectively, and to H₂O forming a linear chain of metal complexes (Figure S27). The core bond distances and angles are similar to the other complexes (Table 2). The pendent diamine groups are in an *anti*-arrangement.

Electrochemical Studies

The cyclic voltammograms (CVs) of Cu-1, Cu-2*, Cu-3, and Cu-4 each display a single quasi-reversible reduction event between 0 to -2 V vs Fc⁺/Fc⁰ (Figure 5). Based on density functional theory studies of Cu(ATSM), the reduction event is associated with a metal centered Cu^{II/I} couple.^[22] To establish that the



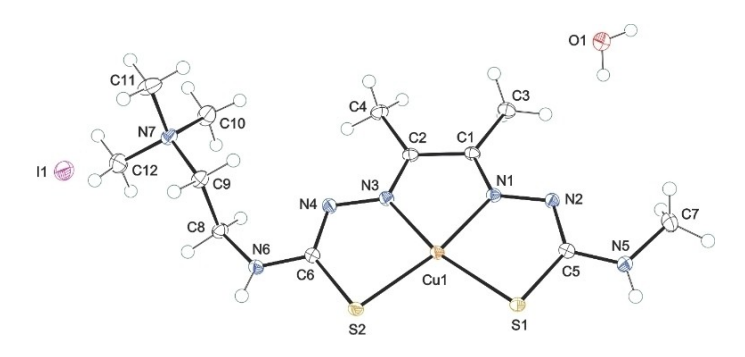


Figure 2. ORTEP view (50% probability ellipsoids) of Cu-2 showing atom labelling for all non-hydrogen atoms in the asymmetric unit.

Figure 3. ORTEP view (50% probability ellipsoids) of **Cu-3** showing atom labelling for all non-hydrogen atoms in the asymmetric unit.

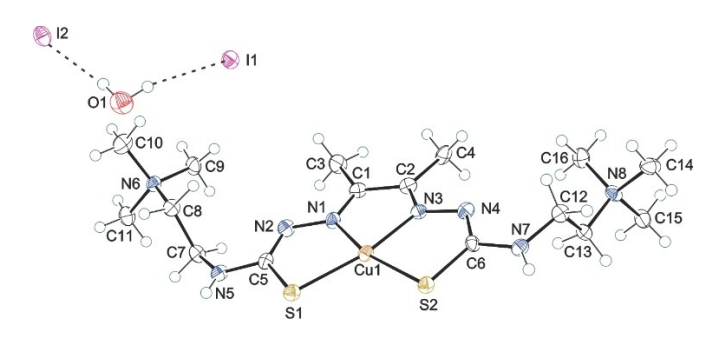


Figure 4. ORTEP view (50% probability ellipsoids) of **Cu-4** showing atom labelling for all non-hydrogen atoms in the asymmetric unit.

reductions are diffusion limited, the CVs were recorded over multiple scan rates from 0.1 to 0.5 V/s. Cottrell plots (Figures S29–S32) of the current data were linear indicating the redox events are diffusion controlled. The experimentally determined diffusion coefficient (D_0) is $1.6\times10^{-5}\,\mathrm{cm}^2\mathrm{s}^{-1}$ for Cu-1, $4.2\times10^{-5}\,\mathrm{cm}^2\mathrm{s}^{-1}$ for Cu-2*, $5.2\times10^{-5}\,\mathrm{cm}^2\mathrm{s}^{-1}$ for Cu-3, and $1.6\times10^{-5}\,\mathrm{cm}^2\mathrm{s}^{-1}$ for Cu-4.

The reduction potentials values of $-1.10\,\mathrm{V}$ and $-1.09\,\mathrm{V}$ for Cu-1 and Cu-3, respectively, match that of Cu(ATSM) indicating addition of the pendent ethyldimethylamine does not significantly perturb the electronic properties of the $\mathrm{CuN_2S_2}$ core (Table 3). This was also observed for the corresponding Ni derivatives with Ni-1 and Ni-3 displaying reduction potentials comparable to Ni(ATSM). Inclusion of fixed charges in the methylated derivatives Ni-2 and Ni-4 was previously shown to shift the potential anodically by 60 mV and 160 mV, respectively, relative to Ni(ATSM) (Table 3). Curiously, Cu-2 displayed

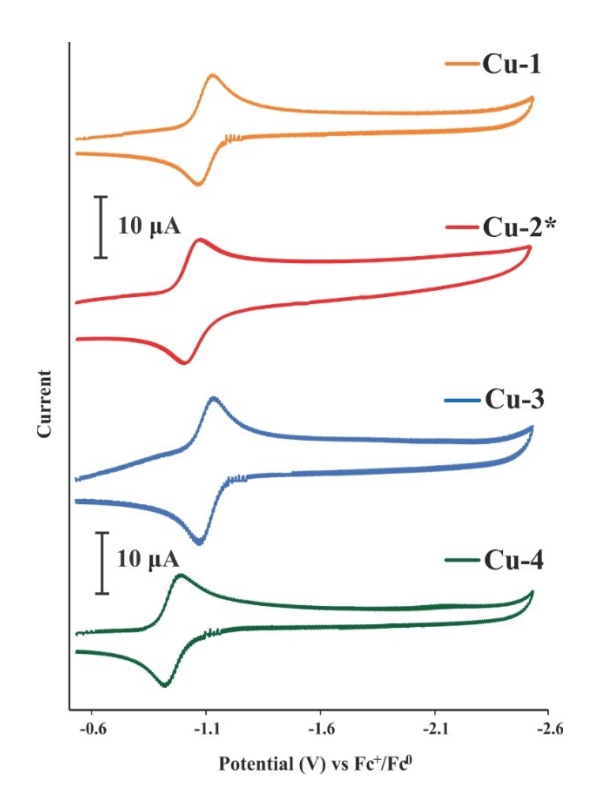


Figure 5. Cyclic voltammograms of 0.3 mM Cu-1, Cu-2*, Cu-3, and Cu-4 recorded in 0.1 M Bu₄NPF₆/MeCN solution at a scan rate of 200 mV/s.

Table 3. Electrochemical data for 0.3 mM of M-1–M-4 (M=Cu or Ni ^[14]) in 0.1 M $Bu_4NPF_6/MeCN$ solution at a scan rate of 200 mV/s with potentials vs. Fc^+/Fc^0 .			
Complex	$Cu^{II}L/Cu^{I}L^{\bullet}E_{1/2}[V]$	$Ni^{\parallel}L/Ni^{\parallel}L^{\bullet} = E_{1/2}, Ni^{\parallel}L^{\bullet} = -/Ni^{\parallel}L^{\bullet 2} = E_{1/2} [V]$	
M(ATSM) M-1 M-2* M-3 M-4	-1.10 -1.10 -1.04 -1.09 -0.94	-1.72, -2.32 -1.72, -2.32 -1.64, -2.24 -1.73, -2.33 -1.57, -2.18	

only a 10 mV shift relative to Cu(ATSM) (Figure S28), while the reduction potential for **Cu-4** was shifted by 160 mV relative to Cu(ATSM). However, the reduction potential for the hexafluor-ophosphate derivative, **Cu-2***, showed the expected 60 mV anodic shift suggesting that ion pairing of the cationic metal complex and iodide of **Cu-2** in acetonitrile yields a charge neutral species. To confirm this, a series of conductivity measurements were conducted using electron impedance spectroscopy (EIS). Complexes **Cu-1** and **Cu-2** have similar conductivity values of 0.054 mS cm⁻¹ and 0.052 mS cm⁻¹, respectively, consistent with ion-pairing in the latter.

Electrocatalytic Hydrogen Evolution Studies

The performance of **Cu-1–Cu-4** as electrocatalysts for the hydrogen evolution reaction (HER) was evaluated in MeCN using glacial acetic acid as a proton source. The addition of CH₃COOH to 0.3 mM solutions of **Cu-1–Cu-4** in MeCN contain-



ing 0.1 M Bu₄NPF₆ generates catalytic current upon a sweep in the cathodic direction (Figures S33-S36). The catalytic current was corrected by subtracting the CVs of acetic acid in the absence of catalyst (Figure 6 and Figures S33-S36). For each complex, the catalytic to peak current ratio (i_{cat}/i_p) increases linearly with the increasing acid concentration until saturation at ~100 mM CH₃COOH (Figure S37). For each catalyst the overpotential was calculated under acid saturated conditions using the methods reported by Fourmond et al. as described in the supporting information. [25,26] The turnover frequency (TOF) for each catalyst was calculated from the plateau currents as described in the supporting information. A comparison of the overpotential and TOF values for Cu-1-Cu-4 with Cu(ATSM) is provided in Table 4. The values for Cu(ATSM) are based on experiments performed during this study and the calculated overpotential is increased relative to the prior report due to a difference in the calculation of E_{ref} ^[22]

As shown in Table 4, the addition of pendent polyamines in Cu-1–Cu-4 reduces the overpotential for HER relative to Cu (ATSM). The overpotential values of 0.65 V and 0.66 V for Cu-1 and Cu-3, respectively are shifted by 120–130 mV relative to Cu (ATSM). This is despite the similarity of the reduction potentials for the three complexes in the absence of substrate. For the charged complexes Cu-2 and Cu-4 the overpotential values of 0.68 V and 0.72 V, respectively, are also more accessible than Cu (ATSM). However, the shifts are smaller than the charge neutral derivatives Cu-1 and Cu-3. Under acid-saturated catalytic conditions all of the catalysts have charged pendent amines either due to protonation, in the case of Cu-1 and Cu-3, or methylation, in the case of Cu-2 and Cu-4. The introduction of

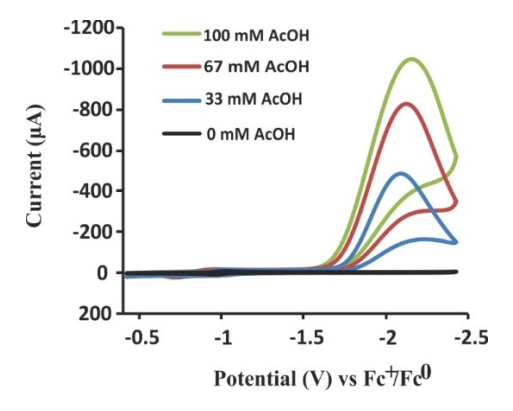


Figure 6. Background acid subtracted cyclic voltammograms of 0.3 mM of Cu-3 recorded in 0.1 M $Bu_4NPF_6/MeCN$ solution with increasing amounts of CH_3COOH .

Table 4. Electrocatalytic HER parameters for 0.3 mM of **Cu-1–Cu-4** under acid saturated conditions (100 mM acetic acid) in MeCN with 0.1 M Bu_4NPF_6 at a scan rate of 200 mV/s. Potentials are referenced versus $Fc^+/Fc = 0.0 \text{ V}$.

Complex	η [V]	$E_{cat/2}$ [V]	TOF [s ⁻¹]	
Cu(ATSM)	0.90	-2.20	9500	
Cu-1	0.64	-1.94	10300	
Cu-2*	0.67	-1.97	9400	
Cu-3	0.65	-1.95	12000	
Cu-4	0.70	-2.00	8700	

charged pendent amines lowers the overpotential by shifting the reduction potential anodically, although this may be partially offset as the positive charge makes the complex more difficult to protonate, which may retard intramolecular proton rearrangement. In addition to charge effects, the protonated pendent amines in **Cu-1** and **Cu-3** can act as proton relays that facilitate intramolecular proton rearrangement and further lower overpotential.

The data in Table 4 highlights the effect of pendent polyamines on the HER TOF for the four copper complexes. The TOF values of $10,300 \, s^{-1}$ and $12,000 \, s^{-1}$ for **Cu-1** and **Cu-3**, respectively, are $108\,\%$ and $112\,\%$ of the value observed for Cu (ATSM). The introduction of pendent amines as proton relays in **Cu-1** and **Cu-3** improves the TOF. The highest TOF was observed for **Cu-3**, which has two such pendent amines. The introduction of charged, pendent amines through methylation decreases TOF. For the charged complexes **Cu-2** and **Cu-4** the TOF values of $9400 \, s^{-1}$ and $8700 \, s^{-1}$ are $99\,\%$ and $92\,\%$ of the Cu(ATSM) TOF.

Electrocatalytic Hydrogen Evolution: CPC Studies

The stability of **Cu-1-Cu-4** as electrocatalysts for HER was evaluated in MeCN by conducting controlled potential coulometry (CPC) experiments over a period of 4 hours (Figure 7). Electrolysis of 0.30 mM MeCN solutions of **Cu-1-Cu-4** containing 0.1 M Bu_4NPF_6 , and 100 mM CH_3COOH were performed at a constant potential of $E_{cat/2}$, defined as the potential required to obtain one-half of the maximum of catalytic current, $i_{cat/2}$, in the CV studies. A plot of charge versus time shows a linear dependence over the entire time of the experiment, indicating the catalyst's stability. For **Cu-1**, a total charge (q) of 30.24 C was passed corresponding to 1.56×10^{-4} moles of H_2 produced (n) and 52 turnovers (Table 5). The greatest activity was

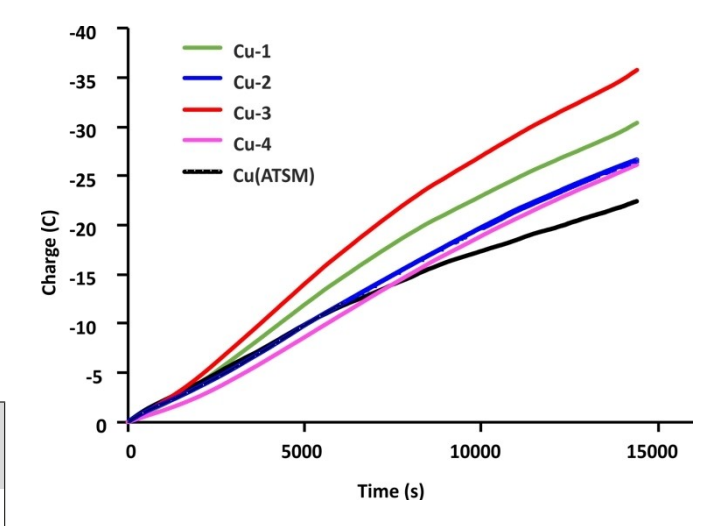


Figure 7. Controlled potential coulometry of 0.3 mM of **Cu-1–Cu-4** and Cu (ATSM) in 0.1 M Bu₄NPF₆/MeCN solutions with 100 mM CH₃COOH. The CPC were performed for **Cu-1–Cu-4** and Cu(ATSM) at -1.5 V vs. Ag/Ag $^+$. The charge generated by the acid blanks in the absence of the catalysts were subtracted.



Table 5. Controlled potential coulometry results.			
Complex	Q [C]	$n \times 10^{-4}$	Turnovers
Cu(ATSM)	23.57	1.22	40
Cu-1	30.24	1.56	52
Cu-2	27.12	1.40	46
Cu-3	35.72	1.85	61
Cu-4	26.35	1.36	45

displayed by **Cu-3**, which catalyzed 61 turnovers during the time of the electrolysis. The charged derivatives **Cu-2** and **Cu-4** catalyzed 46 and 45 turnovers, respectively, which is similar to the 40 turnovers for Cu(ATSM). The change in slope of the Cu (ATSM) sample at ~9000 s may be due to the film formation on the electrode. All of the complexes exhibited faradaic efficiencies of approximately 100% (Figure S39). Extended CPC experiments with **Cu-1** over 24 hours showed no degradation of catalytic activity (Figure. S40).

Post-electrolysis dip-test. To test if proton reduction occurs as the result of the deposition of copper nanoparticles on the electrode surface, a dip-test was performed following CPC studies with Cu-1–Cu-4. After CPC experiments, the working electrode was removed from solution, washed with DI water without being polished, and immersed into a fresh 0.1 M Bu₄NPF₆/MeCN solution. For all complexes, only background current was observed upon sweeping the potential in the cathodic region (Figure S41). Upon addition of acetic acid, only the acid blank was observed (Figure S42). This indicates that HER activity is not due to nanoparticle formation on the electrode.

Conclusion

The HER activity of four copper BTSC complexes with pendent polyamine groups has been evaluated. Complexes **Cu-1** and **Cu-3** contain pendent basic amines, while **Cu-2** and **Cu-4** are their quaternary amine derivatives. In the absence of acid substrate, the introduction of the neutral pendent polyamines does not influence the reduction potentials of **Cu-1** and **Cu-3**, while the introduction of charged sites in **Cu-2** and **Cu-4** shifts the complex reduction potential anodically. However, the effect on HER overpotential is more complicated. The catalytic potential ($E_{\text{Cat/2}}$) does not equal the thermodynamic potential ($E_{\text{1/2}}$) and the shifting of overpotential as a function of scan rate indicates intramolecular proton rearrangement is limiting the rate of HER.^[27,28]

The results are consistent with the proposed CECE path for Cu(ATSM), which includes neutral and cationic species, Scheme 2a. [22] The initial step is protonation. For Cu-1–Cu-4 the data in Table 4 clearly shows a charge effect. The methylated derivatives Cu-2 and Cu-4 have a lower HER overpotential than Cu(ATSM) attributed to tuning of the catalyst reduction potential. Notably, the overpotential for Cu-2 is lower than Cu-4 suggesting that the introduction of the second fixed charge site makes protonation and intramolecular proton rearrangement more difficult. In Cu-1 and Cu-3 the pendent amine acts as a

a)
$$Cu^{II}L \xrightarrow{H^+} [Cu^{II}(HL)]^+$$
 b) $Ni^{II}L \xrightarrow{e^-} [Ni^{II}L^*]^-$

$$\downarrow^{H_2} \downarrow^{H_2} \downarrow^{H^+} \downarrow^{$$

Scheme 2. A) ECEC pathway for Ni(BTSC) catalyzed HER. B) CECE pathway for Cu(BTSC) catalyzed HER.

proton relay to enhance proton rearrangement and HER activity.

In comparison to our prior study on the related nickel derivatives, the copper results show some key differences that stem from the differing HER pathways followed by Cu(ATSM) and Ni(ATSM). The ECEC pathway for Ni(ATSM) alternates between neutral and anionic species, Scheme 2b. [18,21] As previously reported, for Ni-1–Ni-4 there are no discernable charge effects as the HER activity of Ni-2 and Ni-4 are similar to that of Ni(ATSM). The enhanced activity of Ni-1 and Ni-3 results from the ability of the pendent amine to act as a proton relay that lowers the barrier to proton rearrangement.

In summary, the effect of proton relays and charged moieties on the electrocatalytic HER activity of copper BTSC complexes is more complex than their nickel analogues. For nickel, the effect was attributed to the presence of pendent relays that lowered HER overpotential by 70–100 mV. No evidence of charge effects was observed. For copper, the principal effect of the pendent polyamines is related to charge effects, which lower the HER overpotential by 60–100 mV. Notably, increasing the number of charged sites retards the degree of the charge effect, which is attributed to repulsive effects that hinder protonation. The proton relay effect further decreases overpotential by an additional ~30–60 mV. These results demonstrate the various effects of pendent derivatives to tune the activity of metal BTSC electrocatalysts and their dependence on the reaction pathway.

Experimental Section

Physical Methods. Elemental analyses were performed by Midwest Microlab, (Indianapolis, IN, USA). ¹H and ¹³C NMR data were collected on a Varian Inova 500 MHz and Varian 400 MHz NMR Spectrometers in commercial deuterated solvents (Aldrich or Cambridge Isotopes). Matrix assisted laser desorption/ionization (MALDI) was collected by Voyager Biospectrometry DE Workstation (Applied Biosystems, Foster City, CA, USA) and processed by Data Explorer Software TM (Version 4.8) at University of Louisville. The matrix for MALDI experiment was prepared by dissolving 0.18 M p-nitroaniline (PNA) in MeOH: CHCl₃ (1:1) solution. The samples were dissolved in MeCN and 0.75 mL aliquot using the dried-droplet method. All EPR data were collected on powder samples at room temperature using a Bruker EMX X-band spectrometer. Infrared spectra were recorded on a Thermo Nicolet Avatar 360 spectrometer with an ATR attachment (4 cm⁻¹ resolution). Electronic absorption spectra were recorded with an Agilent 8453 diode array spectrometer with a 1 cm path length quartz cell.



Electrochemical Methods

Cyclic voltammetry (CV) and controlled potential coulometry (CPC) experiments were performed using a Gamry Interface potentiostat/galvanostat. Overpotential (η) for hydrogen evolution was calculated using the methods reported by Fourmond et al.^[25] from the theoretical half-wave potential, $E_{1/2}^{T}$, and the experimental potential $E_{cal/2}$, Equation 1.

$$\eta = |E^{T}_{1/2} - E_{cat/2}| \tag{1}$$

The value of $E_{cat/2}$ is defined as the potential required to obtain $i_{cat/2}$, one half of the maximum of catalytic current. The CV data were collected using a three-electrode cell comprised of a glassy carbon working electrode, platinum wire counter electrode, and Ag/Ag⁺ reference electrode. Reported potentials are scaled vs. a ferrocenium/ferrocene (Fc⁺/Fc) standard, which was determined using ferrocene as an internal standard. The glassy carbon working electrode was polished by figure-eight motions on a cloth polishing pad in a water-alumina slurry before recording the data. The working and counter electrodes were washed with water, ethanol, isopropanol, acetone, and MeCN, before use. After the washing, the electrodes were sonicated for 15 minutes in the working solvent (MeCN). The three-neck electrochemical cell used for CV studies was washed and dried in an oven overnight before use. In a typical CV experiment, a 0.3 mM solution of the catalyst was prepared in the working solvent (MeCN) containing 0.1 M tetrabutylammonium hexafluorophosphate (Bu₄NPF₆) as supporting electrolyte. The solution was sparged with nitrogen for ~15 minutes and then kept under a nitrogen atmosphere during data collection.

The CPC data were collected using a two-chambered glass electrolysis cell. The working compartment was fitted with a glassy carbon working electrode and Ag/Ag⁺ reference electrode. The auxiliary compartment was fitted with a graphite counter electrode. The cell was washed and dried in oven overnight before conducting the experiments. In a typical experiment, the working compartment was loaded with 0.3 mM catalyst, CH₃COOH at saturation conditions, and 0.1 M Bu₄NPF₆ in MeCN solution. The auxiliary compartment was filled with a 0.1 M Bu₄NPF₆/MeCN solution. Before electrolysis, both compartments were sparged with nitrogen for 15 minutes and then stirred throughout bulk electrolysis experiment. Data were collected at a constant applied potential equal to the potential required for $i_{cat/2}$ in the CV studies. A control (blank) CPC study was conducted and subtracted from experimental results. Hydrogen gas was measured by gas chromatography (GC, SRI 6810) via online automatic injection (1 mL sample) and a thermal conductivity detector (TCD). Nitrogen (99.99%, Specialty Gases) was used as the carrier gas to enable accurate hydrogen quantification. The gas was injected every 15 minutes and each measured value for faradaic efficiency is representative of the past 15 minutes of electrolysis. In the bulk electrolysis cell itself nitrogen was diffused into the electrolyte at 10 sccm regulated by a mass flow controller (MKS Instruments, Inc.). The electrochemical cell was set up identically as described for all other homogeneous electrochemical experiments except joints were sealed with vacuum grease and a nitrogen outlet line was run from the cell to the GC apparatus. In order to maintain an air-tight seal, the GCE was not rotated. Instead, a magnetic stir was rotated at 360 RPM underneath the GCE to remove hydrogen bubbles from the electrode surface. Theoretical H₂ was determined by counting the coulombs of charge passed, and measured H₂ was determined via GC. The faradaic efficiencies were determined by comparing these values.

Electrochemical impedance spectroscopy (EIS) was carried out on acetonitrile solutions of complexes Cu-1-Cu-4 with a prefabricated spacer with holes that allowed the two platinum wire leads to

remain separated at a fixed distance. Then, running these leads to the working/working sense and counter/reference electrode ports respectively of a Metrohm Autolab PGSTAT128 N potentiostat/galvanostat operating in potentiostatic mode. A direct bias of 0 V was applied, and an alternating bias of $\pm\,10$ mV was applied, starting at a frequency of 100 kHz and ending at 0.1 Hz, taking ten data points per decade of frequency. At each data point, real, imaginary, and combined impedances as well as the phase angle between applied voltage and current response were acquired. Raw impedance data were imported into Zview software where the data points were fitted to an equivalent circuit model using the method of least squares.

Materials and methods. All reagents were obtained from commercially available sources and used as received unless otherwise noted. Commercial solvents were additionally dried and purified using an MBraun solvent purification system unless otherwise noted. The complexes in this study are air and moisture stable as solids and were handled on the benchtop with no additional required protection from the atmosphere.

Synthetic procedures. All reactions were performed open to air and under ambient conditions unless otherwise indicated. The ligands H_3L^1 and H_2L^2 were prepared as previously described.^[14]

Cu-1: To a suspension of H_2L^1 (0.20 g, 0.63 mmol) in MeOH (25 mL) was added $Cu(OAc)_2 \cdot H_2O$ (0.126 g, 0.63 mmol). The resulting redbrown suspension was refluxed with stirring overnight. The brown precipitate was filtered and air dried. Yield = 0.149 g (62%). X-ray quality single crystals were obtained by slow evaporation of a MeCN/EtOH (1:1) solution of Cu-1. FT-IR, cm⁻¹: 3288 (br, m, N–H), 2947 (br, w), 1395 (vs, C=N), 1217 (s, thioamide), 945 (w), 772 (w). UV – vis (MeCN): λ_{max} , nm (ϵ , M^{-1} cm⁻¹) = 324 (39,000), 393 (12,000). Conductivity: 0.052 mS cm⁻¹. Anal. Calc. for $C_{11}H_{21}N_7CuS_2$: C, 34.86; H, 5.58; N, 25.87. Found: C, 34.72; H, 5.39; N, 25.46. + MALDI, m/z calcd for {[$C_{11}H_{21}N_7CuS_2$]-H⁺} 379.07. Found: 379.33.

Cu-2: To a suspension of Cu-1 (0.075 g, 0.198 mmol) in MeCN (10 mL) was added methyl iodide (12 μL , 0.198 mmol). The resulting brown suspension was stirred overnight at room temperature. The brown precipitate was filtered and air dried. Yield = 0.066 g (64%). X-ray quality single crystals were obtained by slow evaporation of a MeCN/EtOH (1:1) solution of Cu-2. FT-IR, cm $^{-1}$: 3286 (br, s, N–H), 2946 (w), 1394(br, vs, C=N), 1218 (s, thioamide), 1084 (w), 917 (w). UV - vis (MeCN): λ_{max} , nm (ϵ , M $^{-1}$ cm $^{-1}$) = 258 (24,000), 325 (42,000), 472 (12,000). Conductivity: 0.054 mS cm $^{-1}$. Anal. Calc. for C $_{12}H_{24}N_7\text{CuS}_2\cdot H_2\text{O}$: C, 26.74; H, 4.86; N, 18.19. Found: C, 26.58; H, 4.52; N, 17.92. + MALDI, m/z calcd for {[C $_{12}H_{24}IN_7\text{CuS}_2]-H^+} 393.08. Found: 393.15.$

Cu-2*: To 20 mL saturated solution of KPF₆ in deionized H₂O a redbrown solution of Cu-2 (0.060 g, 0.115 mmol) in deionized H₂O was added. Upon addition, Cu-2* precipitated as a red-brown solid and was filtered and washed with deionized H₂O (3×5 mL) and then air dried. Yield = 0.059 g (95%). ^{19}F NMR (376 MHz), $d_6\text{-DMSO}$): $\delta\text{/ppm}$ -77.39 (d, J_{FP} = 706 Hz). ^{31}P NMR (162 MHz), $d_6\text{-DMSO}$): $\delta\text{/ppm}$ -149.07 (h, J_{PF} = 706 Hz).

Cu-3: To a clear solution of H_2L^2 (0.200 g, 0.534 mmol) in MeOH (25 mL) was added Cu(acac)₂· H_2O (0.107 g, 0.534 mmol). The resulting red-brown solution was refluxed with stirring for 2 h. Brown precipitate was isolated by addition of diethyl ether, filtered and air dried. Yield = 0.193 g (83%). X-ray quality single crystals were obtained by vapor diffusion of diethyl ether into an acetonitrile solution of **Cu-3.** FT-IR, cm⁻¹: 3336 (br, m, N–H), 2943 (br, m), 2823 (w), 2775 (w), 1415 (vs, C=N), 1215 (s, thioamide), 934 (w), 774 (w). UV – vis (MeCN): λ_{max} nm (ϵ , M⁻¹ cm⁻¹) = 320 (37,000), 462 (11,000). Conductivity: 0.052 mS cm⁻¹. Anal. Calc. for $C_{14}H_{28}N_8CuS_2 \cdot 0.75H_2O$: C, 37.40; H, 6.63; N, 24.93. Found: C, 37.66; H,



6.42; N, 24.75. + MALDI, m/z calcd for {[$C_{14}H_{28}N_8CuS_2$]- H^+ } 436.13. Found: 436.27.

Cu-4: To a suspension of **Cu-3** (0.100 g, 0.229 mmol) in MeCN (15 mL) was added methyl iodide (28.55 μL, 0.459 mmol). The resulting red-brown suspension was stirred overnight at room temperature. Brown precipitate was filtered and air dried. Yield = 0.149 g (90%). X-ray quality single crystals were obtained by slow evaporation of an acetonitrile solution of **Cu-4**. FT-IR, cm⁻¹: 3272 (br, m, N—H), 1410 (vs, C=N), 1228 (s, thioamide), 914 (br, m). UV-vis (MeCN): λ_{max} nm (ε, $M^{-1}\text{cm}^{-1}$) = 263 (36,000), 318 (28,000), 467 (8,000). Conductivity: 0.074 mS cm⁻¹. Anal. Calc. for C₁₆H₃₄I₂N₈CuS₂·1.25H₂O: C, 25.88; H, 4.96; N, 15.09. Found: C, 26.09; H, 4.64; N, 14.75. + MALDI, m/z calcd for {[C₁₆H₃₄N₈CuS₂]-H⁺} 233.2. Found: 233.3

Crystallographic Studies.

A red-brown plate 0.20×0.20×0.01 mm³ crystal of **Cu-1** grown by slow evaporation of a 1:1 solution of acetonitrile/ethanol was mounted on a glass fiber for collection of x-ray data on an Agilent Technologies/Oxford Diffraction Gemini CCD diffractometer. The CrysAlisPro^[29] CCD software package (v 1.171.36.32) was used to acquire a total of 216 frame thirty-second frame ω -scan exposures of data at 102 K to a $2\theta_{\rm max}{=}\,$ 54.44° using monochromated MoK α radiation (0.71073 Å) from a sealed tube. Cu-1 crystallizes in the orthorhombic space group Pbca with unit cell parameters: a = 10.6564(4)Å, b=15.0501(6) Å, c=20.1476(8) Å, $\alpha = \beta = \gamma = 90^{\circ}$, V= 3231.3(2) Å³, Z=8 and D_{calc} = 1.558 Mg/m³. 3,600 independent data were corrected for absorption (transmission min./max. = 0.928/ 1.000; μ =1.614 mm $^{-1}$) using SCALE3 ABSPACK2. [30] The structure was solved by Direct methods using SHELXS.[31] All non-hydrogen atoms were refined with anisotropic atomic displacement parameters. All H's were located by difference maps and refined isotropically. For reflections $I > 2\sigma(I)$ (R(int) 0.060) the final anisotropic full matrix least-squares refinement on F² for 274 variables converged at $R_1 = 0.040$ and $wR_2 = 0.076$ with a GOF of 1.08.

A red-brown plate 0.42×0.20×0.05 mm³ crystal of Cu-2 grown from slow evaporation of a 1:1 solution of acetonitrile/ethanol was mounted on a glass fiber for collection of x-ray data on an Agilent Technologies/Oxford Diffraction Gemini CCD diffractometer. The CrysAlisPro^[29] CCD software package (v 1.171.36.32) was used to acquire a total of 503 fifteen-second frame ω-scan exposures of data at 102 K to a $2\theta_{\rm max}{=}67.20^{\circ}$ using monochromated MoKlpharadiation (0.71073 Å) from a sealed tube. Final unit cell parameters: a = 8.2819(4) Å, b = 29.944(2) Å, c = 8.9097(4) Å, $\alpha = \gamma = 90^{\circ}$, $\beta =$ 115.093(6)°, $V = 2001.03(19) \text{ Å}^3$, $D_{calc} = 1.789 \text{ Mg/m}^3$, Z = 4 to produce raw hkl data that were then corrected for absorption (transmission min./max. = 0.624/1.000; μ = 2.858 mm⁻¹) using SCALE3 ABSPACK2.[30] The structure was solved by Direct methods in the space group $P2_1/n$ using SHELXS^[31] and refined by least squares methods on F² using SHELXL.^[31] Non-hydrogen atoms were refined with anisotropic atomic displacement parameters. All hydrogen atoms (except for methyl H's) were located by difference maps and refined isotropically. Methyl H atoms were placed in their geometrically generated positions and refined as a riding model and these atoms were assigned $U(H) = 1.5 \times Ueq$. For all 7,885 unique reflections (R(int) 0.035) the final anisotropic full matrix least-squares refinement on F² for 305 variables converged at R₁= 0.039 and $wR_2 = 0.060$ with a GOF of 1.08.

A red-brown prism $0.30\times0.17\times0.05~\text{mm}^3$ crystal of **Cu-3** grown by vapor diffusion of diethyl ether into a solution of acetonitrile was mounted on a glass fiber for collection of x-ray data on an Agilent Technologies/Oxford Diffraction Gemini CCD diffractometer. The CrysAlisPro^[29] CCD software package (v 1.171.36.32) was used to

acquire a total of 874 twenty-second frame ω-scan exposures of data at 102 K to a $2\theta_{\rm max}{=}60.36^{\circ}$ using monochromated MoKlpharadiation (0.71073 Å) from a sealed tube. Frame data were processed using CrysAlisPro RED to determine final unit cell parameters: a = 8.8712(3) Å, b = 9.1946(3 Å, c = 12.8507(3) Å, $\alpha =$ 95.544(2)°, $\beta = 106.566(3)$ °, $\gamma = 107.451(3$ °, V = 939.24(5) ų, $D_{calc} = 100.566(3)$ °, V = 100.566(3)°, V = 100.5661.542 Mg/m 3 , Z=2 to produce raw hkl data that were then corrected for absorption (transmission min./max.=0.922/1.000; μ = 1.401 mm⁻¹) using SCALE3 ABSPACK. [30] The structure was solved by Direct methods in the space group P-1 using SHELXS^[31] and refined by least squares methods on F² using SHELXL.^[31] Non-hydrogen atoms were refined with anisotropic atomic displacement parameters. All H's were located by difference maps and refined isotropically. For all 5,554 unique reflections (R(int) 0.033) the final anisotropic full matrix least-squares refinement on F2 for 338 variables converged at $R_1 = 0.028$ and $wR_2 = 0.056$ with a GOF of 1.05

A twinned crystal of Cu-4 suitable for x-ray analysis was grown by slow evaporation from acetonitrile solution. X-ray structural analysis for Cu-4 was performed on a 0.40 × 0.03 × 0.01 mm³ long, thin orange plate on a CryoLoop using a 886 frame, forty second ω -scan data collection strategy at 102 K to a $2\theta_{\text{max}} = 54.68^{\circ}$. Cu-4 crystallizes in the space group P-1 with unit cell parameters: a = 9.3519(5) Å, b=9.7849(4) Å, c=15.2845(8) Å, α =85.659(4)°, β = 73.253(4)°, $\gamma = 81.935(4)$ °, V = 1325.16(11) ų, Z = 2 and $D_{calc} = 1.850$ Mg/m³ 11,440 raw independent data were corrected for absorption (transmission min./max. = 0.796/1.000; μ = 3.335 mm⁻¹) using SCALE3 ABSPACK.[30] The structure was solved by Patterson methods using SHELXS.[31,33] SHELXL HKLF 5 refinement was used for the twinned crystal. All non-hydrogen atoms were refined with anisotropic atomic displacement parameters. Imine H and water H atoms were located by difference maps and refined isotropically. Methyl H and methylene H atoms were placed in their geometrically generated positions and refined as a riding model and these atoms were assigned $U(H) = 1.5 \times Ueg$. For all 11,440 unique reflections (R(int) 0.010) the final anisotropic full matrix leastsquares refinement on F^2 for 293 variables converged at $R_1 = 0.073$ and $wR_2 = 0.174$ with a GOF of 1.13.

Deposition Numbers 2013250 (for **Cu-1**), 2013252 (for **Cu-2**), 2013249 (for **Cu-3**) and 2013251 (for **Cu-4**) contain the supplementary crystallographic data for this paper. These data are provided free of charge by the joint Cambridge Crystallographic Data Centre and Fachinformationszentrum Karlsruhe Access Structures service www.ccdc.cam.ac.uk/structures.

Acknowledgements

This research was supported by the National Science Foundation via the Award CHE-1665136 and CHE-1800245. The authors also acknowledge support from the Conn Center for Renewable Energy Research at the University of Louisville. M. S. M. thanks the Department of Energy (DEFG02-08CH11538) and the Kentucky Research Challenge Trust Fund for upgrade of our X-ray facilities. Authors are grateful to Alexander J. Gupta for his help in conductivity measurements and to Jacob M. Strain for help with faradaic efficiency experiments.

Conflict of Interest

The authors declare no conflict of interest.



Keywords: Copper • Bis(thiosemicarbazone) • Electrocatalysts • Electrochemistry • Structure elucidation

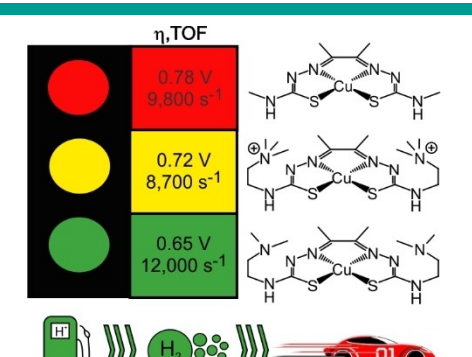
- C. Palopoli, J. Ferreyra, A. Conte-Daban, M. Richezzi, A. Foi, F. Doctorovich, E. Anxolabéhère-Mallart, C. Hureau, S. R. Signorella, ACS Omega 2019, 4, 48–57.
- [2] M. Lanznaster, A. Neves, A. J. Bortoluzzi, A. M. C. Assumpção, I. Vencato, S. P. Machado, S. M. Drechsel, *Inorg. Chem.* 2006, 45, 1005–1011.
- [3] X.-Y. Li, Y.-G. Sun, P. Huo, M.-Y. Shao, S.-F. Ji, Q.-Y. Zhu, J. Dai, Phys. Chem. Chem. Phys. 2013, 15, 4016–4023.
- [4] V. Artero, J.-M. Saveant, Energy Environ. Sci. 2014, 7, 3808–3814.
- [5] S. Sung, D. Kumar, M. Gil-Sepulcre, M. Nippe, J. Am. Chem. Soc. 2017, 139, 13993–13996.
- [6] T. J. Schmeier, G. E. Dobereiner, R. H. Crabtree, N. Hazari, J. Am. Chem. Soc. 2011, 133, 9274–9277.
- [7] I. Azcarate, C. Costentin, M. Robert, J.-M. Savéant, J. Phys. Chem. C 2016, 120, 28951–28960.
- [8] C. Costentin, M. Robert, J.-M. Savéant, Acc. Chem. Res. 2015, 48, 2996–3006.
- [9] C. Costentin, M. Robert, J.-M. Savéant, A. Tatin, Proc. Natl. Acad. Sci. USA 2015, 112, 6882–6886.
- [10] M. Papadakis, A. Barrozo, T. Straistari, N. Queyriaux, A. Putri, J. Fize, M. Giorgi, M. Réglier, J. Massin, R. Hardré, M. Orio, *Dalton Trans.* 2020, 49, 5064–5073.
- [11] I. Azcarate, C. Costentin, M. Robert, J.-M. Savéant, J. Am. Chem. Soc. 2016, 138, 16639–16644.
- [12] A. H. Reath, J. W. Ziller, C. Tsay, A. J. Ryan, J. Y. Yang, *Inorg. Chem.* 2017, 56, 3713–3718.
- [13] K. Kang, J. Fuller, A. H. Reath, J. W. Ziller, A. N. Alexandrova, J. Y. Yang, Chem. Sci. 2019, 10, 10135–10142.
- [14] C. A. Calvary, O. Hietsoi, J. M. Strain, M. S. Mashuta, J. M. Spurgeon, R. M. Buchanan, C. A. Grapperhaus, Eur. J. Inorg. Chem. 2019, 2019, 3782–3790.
- [15] M. Drosou, F. Kamatsos, C. A. Mitsopoulou, Inorg. Chem. Front. 2020, 7, 37–71.

- [16] X. Jing, P. Wu, X. Liu, L. Yang, C. He, C. Duan, New J. Chem. 2015, 39, 1051–1059.
- [17] T. Straistari, R. Hardré, J. Fize, S. Shova, M. Giorgi, M. Réglier, V. Artero, M. Orio, Chem. Eur. J. 2018, 24, 8779–8786.
- [18] T. Straistari, J. Fize, S. Shova, M. Réglier, V. Artero, M. Orio, ChemCatChem 2017, 9, 2262–2268.
- [19] S. Gulati, O. Hietsoi, C. A. Calvary, J. M. Strain, S. Pishgar, H. C. Brun, C. A. Grapperhaus, R. M. Buchanan, J. M. Spurgeon, *Chem. Commun.* 2019, 55, 9440–9443.
- [20] W.-X. Jiang, Z.-L. Xie, S.-Z. Zhan, Inorg. Chem. Commun. 2019, 102, 5-9.
- [21] R. Jain, A. A. Mamun, R. M. Buchanan, P. M. Kozlowski, C. A. Grapperhaus, *Inorg. Chem.* 2018, 57, 13486–13493.
- [22] A. Z. Haddad, S. P. Cronin, M. S. Mashuta, R. M. Buchanan, C. A. Grapperhaus, *Inorg. Chem.* 2017, 56, 11254–11265.
- [23] D. X. West, J. S. Ives, G. A. Bain, A. E. Liberta, J. Valdés-Martínez, K. H. Ebert, S. Hernández-Ortega, Polyhedron 1997, 16, 1895–1905.
- [24] J. L. Dearling, J. S. Lewis, G. E. Mullen, M. J. Welch, P. J. Blower, J. Biol. Inorg. Chem. 2002, 7, 249–259.
- [25] V. Fourmond, P.-A. Jacques, M. Fontecave, V. Artero, *Inorg. Chem.* 2010, 49, 10338–10347.
- [26] V. Fourmond, P.-A. Jacques, M. Fontecave, V. Artero, *Inorg. Chem.* 2015, 54, 704–704.
- [27] K. J. Lee, N. Elgrishi, B. Kandemir, J. L. Dempsey, Nat. Rev. Chem. 2017, 1, 0039
- [28] M. M. Roubelakis, D. K. Bediako, D. K. Dogutan, D. G. Nocera, Energy Environ. Sci. 2012, 5, 7737–7740.
- [29] CrysAlis PRO (CCD and RED), V 1.171.36.32, Agilent Technologies, 2013.
- [30] SCALE3 ABSPACK included in CrysAlis PRO RED, V 171.35.11.
- [31] G. Sheldrick Acta Crystallogr. Sect. A 2008, 64, 112-122.

Manuscript received: August 14, 2020 Revised manuscript received: December 3, 2020

FULL PAPERS

The introduction of pendent amines to copper bis(thiosemicarbazone) complexes enhances electrocatalytic HER activity through second coordination sphere effects. Optimal activity is observed with basic, tertiary pendent amines that serve as proton relays and introduction point charges upon protonation under acid saturated catalytic conditions.



C. A. Calvary, Prof. O. Hietsoi, Dr. D. T. Hofsommer, H. C. Brun, A. M. Costello, Dr. M. S. Mashuta, Prof. Dr. J. M. Spurgeon, Prof. Dr. R. M. Buchanan*, Prof. Dr. C. A. Grapperhaus*

1 – 10

Copper bis(thiosemicarbazone) Complexes with Pendent Polyamines: Effects of Proton Relays and Charged Moieties on Electrocatalytic HER

